J Comput Neurosci
DOI 10.1007/s10827-015-0583-3

# A stochastic model of input effectiveness during irregular gamma rhythms

**Grégory Dumont**[1,2,3] · **Georg Northoff**[2,3] · **André Longtin**[1,3]

Received: 23 March 2015 / Revised: 15 October 2015 / Accepted: 26 October 2015


**Abstract** Gamma-band synchronization has been linked to attention and communication between brain regions, yet the underlying dynamical mechanisms are still unclear. How does the timing and amplitude of inputs to cells that generate an endogenously noisy gamma rhythm affect the network activity and rhythm? How does such "communication through coherence" (CTC) survive in the face of rhythm and input variability? We present a stochastic modelling approach to this question that yields a very fast computation of the effectiveness of inputs to cells involved in gamma rhythms. Our work is partly motivated by recent optogenetic experiments (Cardin et al. *Nature*, *459*(7247), 663–667 2009) that tested the gamma phase-dependence of network responses by first stabilizing the rhythm with periodic light pulses to the interneurons (I). Our computationally efficient model E-I network of stochastic two-state neurons exhibits finite-size fluctuations. Using the Hilbert transform and Kuramoto index, we study how the stochastic phase of its gamma rhythm is entrained by external pulses. We then compute how this rhythmic inhibition controls the effectiveness of external input onto pyramidal (E) cells, and how variability shapes the window of firing opportunity. For transferring the time variations of an external input to the E cells, we find a tradeoff between the phase selectivity and depth of rate modulation. We also show that the CTC is sensitive to the jitter in the arrival times of spikes to the E cells, and to the degree of I-cell entrainment. We further find that CTC can occur even if the underlying deterministic system does not oscillate; quasicycle-type rhythms induced by the finite-size noise retain the basic CTC properties. Finally a resonance analysis confirms the relative importance of the I cell pacing for rhythm generation. Analysis of whole network behaviour, including computations of synchrony, phase and shifts in excitatory-inhibitory balance, can be further sped up by orders of magnitude using two coupled stochastic differential equations, one for each population. Our work thus yields a fast tool to numerically and analytically investigate CTC in a noisy context. It shows that CTC can be quite vulnerable to rhythm and input variability, which both decrease phase preference.

**Keywords** Gamma oscillations · Stimulus selection · Communication through coherence

Action Editor: Frances K. Skinner

✉ Grégory Dumont
gdumont@uottawa.ca

Georg Northoff
georg.northoff@theroyal.ca

André Longtin
alongtin@uottawa.ca

[1] Physics Department, 150 Louis Pasteur Ottawa, Ottawa, Ontario K1N 6N5, Canada

[2] Mind, Brain Imaging and Neuroethics, Royal Ottawa Healthcare, Institute of Mental Health Research, Ottawa, Canada

[3] Center for Neural Dynamics, University of Ottawa, Ottawa, Canada

## 1 Introduction

Gamma-band rhythmicity (30-90 Hz) has been well-documented in many brain regions across many species

Published online: 26 November 2015

(Buzsàki 2006). It has been recorded in the visual cortex (Engel et al. 1991), in the auditory cortex (Brosch et al. 2002), and in the hippocampus (Csicsvari et al. 2003), to mention just a few studies. Research has revealed its existence in non-human mammals (Fries et al. 2001), humans (Schoffelen et al. 2005), and also in insects (Stopfer et al. 1997). It has been associated with many cognitive tasks (Buzsàki 2006), and has been suggested to play a crucial role in attention and routing of information (Fries et al. 2007; Tiesinga and Sejnowski 2009; Sejnowski and Paulsen 2006; Salinas and Sejnowski 2001). However, the precise computational role of gamma-band synchronization (as well as other frequency bands) is still a subject of debate (Sejnowski and Paulsen 2006; Cannon et al. 2014).

There is much evidence that gamma rhythms arise from the interplay between the pyramidal cells (E-cells) and interneurons (I-cells). In this scenario (Buzsáki and Wang 2012; Bartos et al. 2007), there is no need for pacemaker cells to initiate the rhythm; rather, it emerges at the network level due to the synaptic interactions. The rhythm arises as follows: under an external influence, such as a constant background bias, the pyramidal cells start firing spontaneously and excite the interneurons. Once the interneurons activate, they shut down the pyramidal neurons. This leads to a drop in drive to the inhibitory neurons, and the resulting spontaneous re-excitation of the pyramidal cells initiates the cycle anew. This mechanism is referred to as the PING model (Pyramidal Interneuron Network for Gamma oscillation); see for example (Buzsáki and Wang 2012; Bartos et al. 2007) for reviews on the emergence of gamma rhythms, and see also (Wang and Buzsáki 1996; Brunel and Hakim 1999; Lindner et al. 2005; Brunel 2000) for computational implementations.

The particular constitution of the cycle makes the gamma rhythm a good candidate for cortical computations. For example, it has been suggested that the I-cells cyclically gate the availability of the E-cells to fire to external input. In other words, the interneurons periodically modulate the E-cell excitability, all the while being an essential intrinsic component of the rhythm. Since any phase of the gamma cycle is linked to the current degree of inhibition, one expects the ongoing phase to be a temporal marker of network excitability (Fries 2005). The rhythmic inhibition would create consecutive windows of opportunity where synaptic input arriving in an open or "excitable window" has a greater likelihood of inducing a response.

Sequences of open and closed windows of excitability may be central for communication across neural circuits. The communication through coherence hypothesis (CTC) states that, in order to send information to a neural (pyramidal) group oscillating in the gamma frequency, this information should arrive during this window of opportunity. To do so, the source of the information needs to oscillate at the same frequency and remain phase locked to the receiver (Fries 2005; Fries et al. 2007). Neural populations could communicate efficiently with each other when there is a "good" phase relation between the source in one region and the receiver in another. A change in the phase relation between the source and receiver will reflect changes in the information transfer between their neurons. The coupling strength between two brain regions and the presumed ability to share information is thus modulated by the phase relationship, which tunes the effectiveness of inputs at altering activity. Such predictions were verified experimentally as well as using computational modeling approaches (Buehlmann and Deco 2010; Womelsdorf et al. 2007; Tiesinga and Sejnowski 2010; Knoblich et al. 2010).

CTC hypothesizes that an input is expected to be most efficient when it arrives far away from the inhibitory peak. It is however difficult to test this "phase" or timing prediction in CTC, and to further formulate expectations for the role of the stimulus amplitude, without somehow artificially locking the fluctuating rhythm with an external periodic drive. Indeed, since the gamma cycle is noisy in both amplitude and phase, it would be nearly impossible to target the downstream pyramidal cells at a precise desired phase of the ongoing gamma cycle. This problem was circumvented using the clever experimental setup of Cardin et al. (Cardin et al. 2009). In their paper, they entrain the I cells using optogenetic stimulation, and then excite an E cell at different phases of the global gamma rhythm. They conclude, under these "stabilized conditions", that the effectiveness (or "gain") of a stimulus to increase E cell firing depends on its precise timing, lending further support to the CTC hypothesis.

But they leave open some important dynamical questions about the extrinsic and intrinsic factors governing the modulation of input effectiveness. What shapes the dependence of the E cell response on the synchronization of the I cells? Does this shape depend on the intrinsic spontaneous activity of the E and I cells? Does CTC weaken when the rhythms are variable, and the inputs jittered in time? How does it depend on the amplitude of the stimulus to the E-cells? This latter question is pertinent to the biophysically plausible scenario where the amplitude - rather than just the phase- of signals between communicating populations is time-varying, as different numbers of presynaptic cells are recruited over time. And can one have an analytical handle on all this? Apart from these specific questions, our study more generally explores the relation between random spontaneous activity, the fluctuations in the excitatory-inhibitory balance and evoked responses, which are issues related to rest-stimulus interactions, see chapter 10 in (Northoff 2014).

Our computational approach below sheds light on these questions. We use the fully stochastic version of the Wilson-Cowan model on which recent studies have focussed (Wallace et al. 2011) and (Benayoun et al. 2010) and (Buice and Cowan 2007). This model consists of binary neural units that follow a random walk between two possible states, one active and one silent. The behaviour of this model is one that exhibits fluctuations due to finite-size effects; it is known to converge to the standard deterministic Wilson-Cowan model in the thermodynamic mean field limit of an infinite number of cells (Buice and Cowan 2007; Bressloff 2009, 2010; Bressloff and Newby 2013). Furthermore that network model, which can be simulated much faster than networks of integrate-and-fire or Hodgkin-Huxley-type neurons, is known to nicely reproduce many statistical attributes of the gamma cycle (Benayoun et al. 2010). And it can be described succinctly by a pair of stochastic ordinary differential equations, from which certain properties can be computed and on which analytical work can be performed. We show that the resulting system provides a quick computational tool to explore the different biophysical regimes of activity and information transfer in the set-up of Cardin et al. (2009), and in particular to explore the important question of the effect of variability on CTC.

The paper first describes in the Methods section the stochastic spiking process as well as the different measures used to analyze the data produced by the model. It goes on to show how the PING model without external pacing exhibits an endogenous window of opportunity for the E cells. It then explains how this window is constituted by the fluctuating balance of excitation and inhibition. Extending this model to the externally paced I-cells and externally excited E-cells reproduces the main observation of a window of opportunity for CTC in (Cardin et al. 2009) in spite of the fluctuations. The paper then highlights the role of stimulus amplitude, revealing a trade-off between the sharpness in firing phase and the absolute change in firing rate as a result of amplitude changes. In other words a larger change in rate comes with a loss in timing accuracy. It also investigates how jitter in the timing of inputs to the E-cells, the synchronization index of the I cells, and the existence of a deterministic oscillation impact the window of opportunity. And it addresses the resonances seen in the I vs E cells under pacing stimuli delivered to the I vs E cells, supporting the predominant role of the former for rhythm maintenance. The paper ends with a discussion about the implications of our findings, in particular the increase in simulation speed and availability of simple stochastic differential equations for the reduced system that describes the behaviour of the whole network.

## 2 Methods

In this section, we give the details of the mathematical model, its relation to the Wilson-Cowan oscillator and the different measures used in this paper. We first summarize in Table 1 the main mathematical notations and their associated biophysical meaning used throughout this document.

### 2.1 Stochastic spiking process

We first describe the stochastic spiking process based on the Wilson-Cowan equation (Wilson and Cowan 1972). This model is used here to mimic a cortical circuit as

**Table 1** Main notation used throughout this paper and their biophysical interpretation

| Notation | Biophysical interpretation |
|---|---|
| $m$ / $n$ | Number of active inhibitory/excitatory neurons |
| $h_I$ / $h_E$ | Baseline input of inhibitory/excitatory neurons |
| $s_I$ / $s_E$ | Synaptic input of inhibitory/excitatory neurons |
| $w_{IE}$ / $w_{II}$ | Synaptic strengh in inhibitory neurons |
| $w_{EI}$ / $w_{EE}$ | Synaptic strengh in excitatory neurons |
| $\alpha_I$ / $\alpha_E$ | Membrane time constant of inhibitory/excitatory neurons |
| $f(s)$ | Response or "firing rate" function |
| $\beta_I$ / $\beta_E$ | Response function weight of inhibitory/excitatory neurons |
| $r_I$ / $r_E$ | Global inhibitory/excitatory activity |
| $I_I$ / $I_E$ | External drive on inhibitory/excitatory neurons |
| $Q_I$ / $Q_E$ | Amplitude of the external drive on inhibitory/excitatory neurons |
| $\sigma_I$ / $\sigma_E$ | Variance of the external drive on inhibitory/excitatory neurons |
| $T_I$ / $T_E$ | Periode of the external drive on the inhibitory/excitatory neurons |
| $\phi_E$ | Phase shift of the external drive on the excitatory neurons |

presented in (Benayoun et al. 2010). The stochastic version of the Wilson-Cowan equation was introduced to go beyond the usual mean field approximation by taking into account the second order firing statistics, see (Buice and Cowan 2007; Bressloff 2009). The model offers a good framework for our study since it nicely reproduces the main attributes of gamma oscillations (Wallace et al. 2011). A similar approach based on binary neurons to study the spike train correlation of the asynchronous state can be found in (Ginzburg and Sompolinsky 1994), see also (Renart et al. 2010; Helias et al. 2014; Grytskyy et al. 2013) for more recent discussions on spike train correlations.

The population is assumed to be composed of $N_E$ excitatory cells (E-cells) and $N_I$ inhibitory cells (I-cells). It is commonly accepted that a cortical circuit is constituted of 80 percent of E-cells and 20 percent of I-cells. In the stochastic Wilson-Cowan model, each neuron is characterized by a random walk between two possible states (active vs silent). When a neuron enters the active state, it is said to fire an action potential. The transition rates from one state to another of this Markov process are chosen such that the standard Wilson-Cowan model (Wilson and Cowan 1972) is recovered in the thermodynamic mean-field limit (i.e. infinite number of cells), see (Buice and Cowan 2007; Bressloff 2009). During a short interval of time $(t, t + dt)$ the probability that a neuron jumps from the active state to the silent state is $\alpha dt$, see Fig. 1. In other words,

$$\mathcal{P}(\text{active} \to \text{silent, during } dt) = \alpha dt.$$

In the opposite direction from the silent state to the active one, the transition rate depends on the synaptic input $s$ that the neuron receives. The probability that a neuron jumps from the silent state to the active state is calculated using the nonlinear sigmoid response function $f$ and the synaptic input $s$, see Fig. 1

$$\mathcal{P}(\text{silent} \to \text{active, during } dt) = \beta f(s) dt,$$

where the response function $f$ is

$$f(s) = \frac{1}{1 + e^{-s}}. \tag{1}$$

Let $m$ denote the number of active neurons in the excitatory population at a certain time, and $n$ the number of active neurons in the inhibitory population. Assuming an all-to-all coupling, the synaptic input to the excitatory neurons is given by

$$s_E = w_{EE} m/N_E - w_{EI} n/N_I + h_E,$$

and by

$$s_I = w_{IE} m/N_E - w_{II} n/N_I + h_I,$$

for the inhibitory neurons. In the two last mathematical expressions, $h_E$ stands for the external influence or "drive" on the E-cells, and $h_I$ on the I-cells. The synaptic strengths of connection are denoted by $w$. Notice that the model is built under the assumption that the network is perfectly homogenous with all-to-all coupling, see (Wallace et al. 2011) for the influence of sparse connectivity. Following the important remark in (Benayoun et al. 2010), we chose in all our simulations $\alpha_E = 0.1$, which corresponds to a time constant of $\alpha_E^{-1} = 10ms$. Since the basket cells are much faster, we chose $\alpha_I = 0.2$ corresponding to a time constant of $\alpha_I^{-1} = 5ms$. The parameters are similar to those in (Benayoun et al. 2010).

### 2.2 The Wilson-Cowan oscillator

As we mentioned above, the Markov process was first presented to go beyond the usual mean field rate approximation. A first description using the path integral formalism can be found in (Buice and Cowan 2007), and a comparison with Van Kampen's system size expansion is done in (Bressloff 2009) and (Buice and Chow 2013). To speed up the computational performance of the Markov process

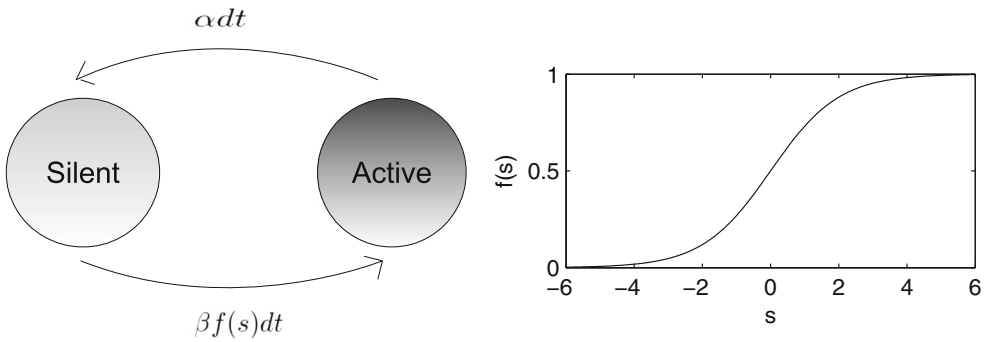


**Fig. 1** The *left* panel is a schematic representation of the random walk between the two possible states (active and silent). During a short interval of time $(t, t+dt)$, a neuron that is in the active state has probability $\alpha dt$ to jump into the silent state, and similarly, a probability $\beta f(s)dt$ to jump from the silent state into the active state, where $f$ is the response function (1) and $s$ the synaptic input. The *right* panel is a graphical representation of the response function $f$

in chemical reactions, the $\tau$-leaping formula was introduced in (Gillespie 2001), see also (Gillespie 2007) for more recent review. The $\tau$-leaping formula can be used to derive a stochastic differential equation, see (Wallace et al. 2013; Wallace 2010; Wallace et al. 2011). It is known that this Markov process can be described by a master equation, and can lead to the Wilson-Cowan equations. Our primary interest is in tracking the statistics of the neural network. The full population of neurons can be described using a master equation. Let $T$ denote $T(t,m,n)$ the probability that the network has the configuration described by $m$ neurons in the active state out of the $N_E$ excitatory cells and $n$ out of the $N_I$ inhibitory. We then have:

$$\begin{aligned}\frac{d}{dt}T(t,n,m) &= \alpha_E\left((m+1)T(t,m+1,n)-mT(t,m,n)\right)\\ &+(N_E-(m-1))\beta_E f(s(m-1,l))T(t,m-1,n)\\ &-(N_E-m)\beta_E f(s(m,n))T(t,m,n)\\ &+\alpha_I\left((n+1)T(t,m,n+1)-nT(t,m.n)\right)\\ &+(N_I-(n-1))\beta_I f(s(m,n-1))T(t,m,n-1)\\ &-(N_I-n)\beta_I f(s(m,n))T(t,m.n). \qquad (2)\end{aligned}$$

To clarify the dynamics of the stochastic spiking process, we compute the first moment. We will derive a moment hierarchy from our master Eq. (2), and then show how it can be truncated. Let us introduce the notation of the first moment

$$< n >= \sum_{n,m} nT(t,n,m).$$

To get an equation for the first moment $< n >$, we multiply the master Eq. (2) by $n$ and sum over all configurations. Algebraic manipulations yield the dynamics of the first moment:

$$\frac{d}{dt} < m >= -\alpha_E < m > +\beta_E < (N_E-m)f(s_E) > .$$

In the limit of infinite neural network size, systems of deterministic differential equations may be derived to describe the expected value of each cells. The most common analytical approach for dynamics on complex networks is mean-field (MF) theory. In this thermodynamic limit, the mean field approximation neglects the correlation among cells. The MF assumption is namely

$$< (N_E-m)f(s_E) >=\simeq (N_E- < m >)f(< s_E >).$$

Of course, the situation for inhibitory cells can be treated in a similar way. Noting

$$r_E =< m > /N_E \quad \text{and} \quad r_I =< n > /N_I,$$

the equation reduces to the standard rate model

$$\begin{cases}\frac{d}{dt}r_E = -\alpha_E r_E + (1-r_E)\beta_E f(s_E)\\ \frac{d}{dt}r_I = -\alpha_I r_I + (1-r_I)\beta_I f(s_I),\end{cases} \qquad (3)$$

where the synaptic inputs are

$$s_E = w_{EE}r_E - w_{EI}r_I + h_E,$$

and

$$s_E = w_{IE}r_E - w_{II}r_I + h_I.$$

The rate model (3) is a good approximation only in the thermodynamic limit $N_E, N_I \to \infty$ and the correlation among cells can be neglected. The deterministic approach regards the time evolution as a continuous, wholly predictable process governed by a set of coupled, ordinary differential equations that neglect correlations among cells. However, the time evolution of binary neurons interacting together is not a continuous process, because the state of each individual cell can change only in a discrete manner. It is possible to show that for finite $N_E$ and $N_I$ that the network is described by stochastic versions of (3), where the noise arises due to finite-size effects. The deterministic Wilson-Cowan equations and the stochastic full network simulations are compared in Fig. 2.

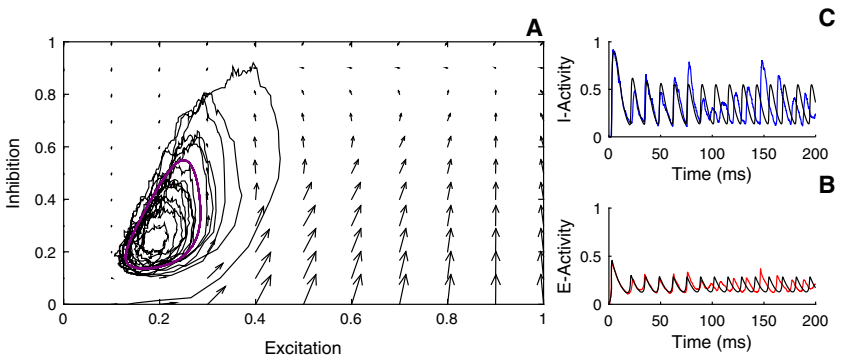


**Fig. 2** Illustration of the gamma rhythm as a stochastic limit cycle. In panel A, the *black line* represents the stochastic trajectory of the normalized (divided by the total number of cells) Markov process. The panels B and C compare, respectively, the stochastic activity generated via the binary cortical network and the deterministic counterpart of the Wilson-Cowan Eq. (3). Parameters for the simulation are as in Fig. 5. The *purple line* indicates the limit cycle

The finite size fluctuations can be added to the equation via a Kramers-Moyal expansion of the master equation (see Bressloff 2009 for details). Using the rescaled variable $r_E$ and $r_I$, and treating them as continuous variables, a Taylor expansion to second order in $1/N$ leads to the Fokker-Planck equation

$$\begin{aligned}\frac{\partial}{\partial t}p(t,r_E,r_I)+\frac{\partial}{\partial r_E}\left((\alpha_E r_E-(1-r_E)\beta_E f(s_E))\,p(t,r_E,r_I)\right)\\ -\frac{1}{N_E}\frac{\partial^2}{\partial r_E^2}\left((\alpha_E r_E+(1-r_E)\beta_E f(s_E))\,p(t,r_E,r_I)\right)\\ +\frac{\partial}{\partial r_I}\left((\alpha_I r_I-(1-r_I)\beta_I f(s_I))\,p(t,r_E,r_I)\right)\\ -\frac{1}{N_I}\frac{\partial^2}{\partial r_I^2}\left((\alpha_I r_I+(1-r_I)\beta_I f(s_I))\,p(t,r_E,r_I)\right)=0 \quad (4)\end{aligned}$$

The solution to the FP Eq. (4) determines the probability density function for a corresponding Ito stochastic process. By a direct application of the Feynman-Kac formula that establishes the link between the FP equation and and stochastic differential equations (see Bressloff 2009 for details), we get that the our stochastic process evolves according to the stochastic Wilson-Cowan model

$$\begin{cases}\frac{d}{dt}r_E=-\alpha_E r_E+(1-r_E)\beta_E f(s_E)+\sqrt{\frac{\alpha_E r_E+(1-r_E)\beta_E f(s_E)}{N_E}}\eta_E(t)\\ \frac{d}{dt}r_I=-\alpha_I r_I+(1-r_I)\beta_I f(s_I)+\sqrt{\frac{\alpha_I r_I+(1-r_I)\beta_I f(s_I)}{N_I}}\eta_I(t).\end{cases} \quad (5)$$

Here $\eta_E(t)$ and $\eta_I(t)$ denote two independent white noises such that

$$\langle\eta(t)\rangle=0,\quad \langle\eta(t)\eta(t')\rangle=\delta(t-t').$$

### 2.3 Power spectrum

To analyze the dynamics of the cortical circuit, we apply some techniques of signal processing. We use the power spectrum measure to quantify the strength of the oscillation of the global gamma activity. We compute the power spectrum via the Fourier transform

$$P(\omega):=\lim_{T\to\infty}\frac{<|\hat{r}(\omega)|^2>}{T},$$

where $\hat{r}(\omega)$ stands for the Fourier transform of the neural activity $r(t)$, and $T$ is the measurement (i.e. simulation) time

$$\hat{r}(\omega)=\int_0^T r(t)e^{-i\omega t}\,dt.$$

The nature of the spectrum of the neural activity gives useful information about its nature, for example, about its degree of periodicity. The result presented in Fig. 2 shows a clear peak in the gamma range.

### 2.4 Phase extraction

It is possible to go beyond the power spectrum to reveal deeper features of the rhythm by computing its phase via a Hilbert transform, which in turn can be used to quantify the instantaneous frequency (see Boashash 1992), which fluctuates even during one gamma cycle. We first apply a bandpass filter to the summed E and I activities $r(t)=r_E(t)+r_I(t)$ that keeps only the $\gamma$-part $r_\gamma(t)$ of the signal. To do so we used the butterworth filter function in the Matlab signal processing toolbox. We chose to use a second order filter, and the lower and upper cutoff frequencies were given by the gamma frequency band $(30-90$ Hz). Such a function allows to design a bandpass in the frequency band of interest. Other definitions of the activity used to compute a global phase will yield qualitatively similar results. Then we write this $\gamma$-part as

$$r_\gamma(t)=E(t)\cos\theta(t).$$

The phase $\theta(t)$ can be extracted via the Hilbert transform $\tilde{r}_\gamma(t)$ of the neural activity signal. We can then compute the analytic signal

$$E(t)e^{i\theta(t)}=r_\gamma(t)+i\tilde{r}_\gamma(t).$$

The phase is extracted via this last formula. An illustration of our method is given in Fig. 6 presented in the Results section. Our methodology illustrates how one can extract the ongoing phase as well as the envelope of the neural network activity in any oscillatory band of interest. Note that from Fig. 6, we see that the reconstructed signal and the original signal are in excellent agreement.

### 2.5 Synaptic drive

To test the excitability of the pyramidal cells as well as to lock the cortical network, we use an external stimulus. In our numerical experiment, we chose a rhythmic drive analogous to (Börgers and Kopell 2008) which has the form

$$I_I(t)=Q_I\sum_{k=-\infty}^{+\infty}\frac{T_I}{\sqrt{2\pi\sigma_I^2}}\exp\left(-\frac{(t-kT_I)^2}{2\sigma_I^2}\right). \quad (6)$$

where $T_I$ is the oscillation period of the rhythmic drive, $\sigma_I$ the width of the input, and the drive frequency is given by

$$f_I=\frac{1000}{T_I}.$$

The factor of 1000 is necessary because we read $T_I$ as a period in $ms$ but keep the frequency $f_I$ to be in Hz. The consequence of such a rhythmic drive is the entrainment of the cortical network's activity as illustrated in Fig. 9. To test the excitability of the pyramidal cells, we shift the periodic

drive on the E-cells relatively to the periodic drive that the I-cells receive:

$$I_E(t) = Q_E \sum_{k=-\infty}^{+\infty} \frac{T_E}{\sqrt{2\pi\sigma_E^2}} \exp\left(-\frac{(t-(k+\frac{\phi_E}{2\pi})T_E)^2}{2\sigma_E^2}\right).$$

This time the phase shift $\phi_E$ allows to test the excitability of the pyramidal cells with respect to the ongoing phase of the gamma cycle as illustrated in Figs. 12 and 13.

To further test the influence of the irregularity of the periodic drive in a more realistic setting, we introduced a gaussian fluctuation in the arrival time of pulses, using a stimulus defined as:

$$I_E(t) = Q_E \sum_{k=-\infty}^{+\infty} \frac{T_E}{\sqrt{2\pi\sigma_E^2}} \exp\left(-\frac{(t-(k+\frac{\phi_E}{2\pi}+\sigma_\eta\eta_k)T_E)^2}{2\sigma_E^2}\right),$$

where $\eta_k$ is a N(0,1) random number:

$< \eta_k \eta_k' >= \delta_{kk'}$.

As above, the phase shift $\phi_E$ allows to test the excitability of the pyramidal cells with respect to the ongoing phase of the gamma cycle, however the phase onset is no longer precise. A small fluctuation deviates the phase stimulus onset with a deviation proportional to $\sigma_\eta$. The illustration on the shape of the stimulus is given in Fig. 3.

### 2.6 Phase locking value

We introduce the phase locking value based on the Kuramoto parameter that we used to quantify the entrainment of the neural network:

$$K = \frac{1}{M}|\sum_{k=1}^{M} e^{i\theta_k}|, \tag{7}$$

where $\theta_k$ is the phase of the neural activity at the stimulus onset, and $M$ the number of stimulus presentations. From its definition, the Kuramoto index is a value between zero and one, a value close to zero for a poor entrainment (weak phase locking), and close to one for strong entrainment (strong phase locking). The result is shown in Fig. 10, where the Kuramoto parameter is shown with respect to the stimulus amplitude.

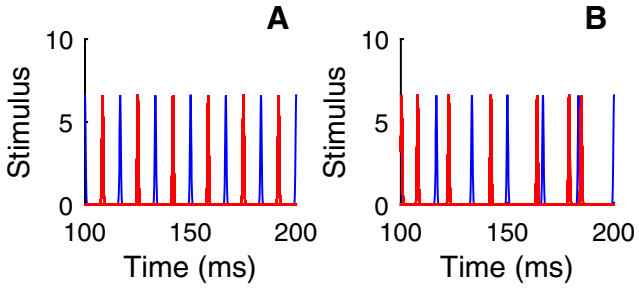


**Fig. 3** Illustration of the influence of noise on the phase target onset. Parameters for the external drive on I-cells are $Q_I = 0.3$, $\sigma_I = 0.3$ and $f_I = 60$; the external drive on E-cells uses $Q_E = 0.3$, $\sigma_E = 0.3$ and $f_E = 60$. **a** $\sigma_\eta = 0$. **b** $\sigma_\eta = 0.3$

## 3 Result

### 3.1 Gamma band synchronization

In this section, we illustrate the gamma rhythm arising from the PING interaction (see Fig. 4) with a simulation of a cortical circuit made up of pyramidal cells and fast basket cells. The model is detailed in the Methods section. Note that there is no external pacing of the I-cells here, as our goal is first to expose any window of opportunity in the fluctuating endogenous gamma rhythm. The neural dynamics is displayed in Fig. 5. We see from the network raster plots that both the E and I-cell populations are globally (i.e. all) engaged in rhythmic behaviour. The spontaneously emerging oscillatory regime is clearly seen by looking at the activity time series (number of active cells per unit of time) and its associated power spectrum. The dominant frequency of the power spectrum is in the gamma band regime (30–90 Hz). Note also that the populations of E-cells and I-cells have similar power spectra. We refer the interested reader to (Kukjin Kang et al. 2010; Mazzoni et al. 2008) for the relation between the low-frequency part of these spectra and local field potential data.

What are the firing patterns in the PING scenario? The pyramidal cells start firing and switch on the fast basket cells. This firing activity can be seen as "spontaneous" even though it relies on a minimum mean level of external activity impinging on the cells; it is not e.g. temporally locked as a response to some external pattern of stimulation. Once these interneurons are activated, they inhibit the pyramidal cells. When the pyramidal cells recover after the decrease of

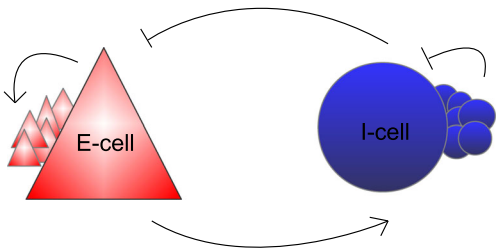


**Fig. 4** Schematic representation of the synaptic interaction between cells in the PING mechanism of gamma rhythm generation. The pyramidal cells (E-cells in *red*) drive the fast basket cells (I-cells in *blue*) that inhibit the whole network. In our computational model, we assume an all-to-all connectivity among cells, and the synaptic interaction is made via a sigmoidal transfert function (1). The details are given in the Method section

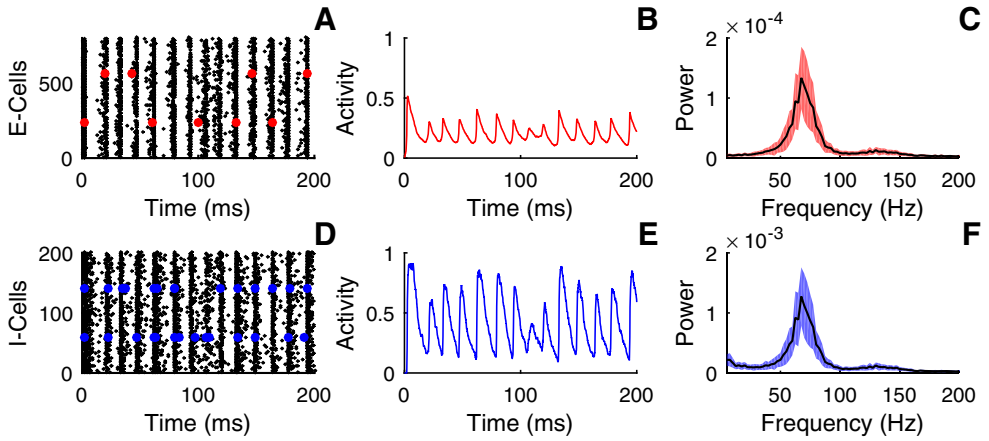


**Fig. 5** Illustration of the PING dynamics. Simulation of the binary Markov network with a cortical circuit composed of 80 percent of E-cells and 20 percent of I-cells during 200 ms. **a** Raster plot depicting the spike timing for the E-cells. **b** Activity (number of active E-cells) as a function of time. **c** Power spectrum computed by averaging over 100 realizations or "trials", which shows a clear peak in the gamma frequency band (30-90 Hz). Similarly, **d, e** and **f** are the corresponding plots for the I-cells. Parameters for the simulation are the number of neurons $N_E = 800$ and $N_I = 200$, the synaptic weights $w_{EE} = 25$, $w_{II} = 1.5$, $w_{IE} = 32$ and $w_{IE} = 18$, the time constants $\alpha_E = 0.1$ and $\alpha_I = 0.2$, $\beta_E = 1$, $\beta_I = 2$ and the external drives $h_E = -3.8$ and $h_I = -9.2$

the inhibitory feedback, the gamma cycle starts again. Note that a given pyramidal cell does not fire at every cycle of the gamma rhythm. This is difficult to see for all cells at the level of resolution of Fig. 5, so the firing times of two specific E cells and two specific I cells are shown in panels A and D, respectively. A cell often misses several cycles of the global oscillation before being able to initiate its next action potential. Consequently this type of gamma rhythm is often called "weak" PING, and has been associated with attentional processing (Cannon et al. 2014). In contrast, a given fast basket cell may fire twice during the same cycle.

From a mathematical perspective, the oscillatory regime can be suitably characterized using mean field theory and dynamical system analysis. Indeed, one can show that in the thermodynamic limit, the Markov walk process (see Methods) used here to simulate the cortical circuit reduces to the well-known Wilson-Cowan equations

$$\begin{cases} \frac{d}{dt} r_E(t) = -\alpha_E r_E(t) + (1 - r_E(t))\beta_E f(s_E(t)) \\ \frac{d}{dt} r_I(t) = -\alpha_I r_I(t) + (1 - r_I(t))\beta_I f(s_I(t)), \end{cases}$$

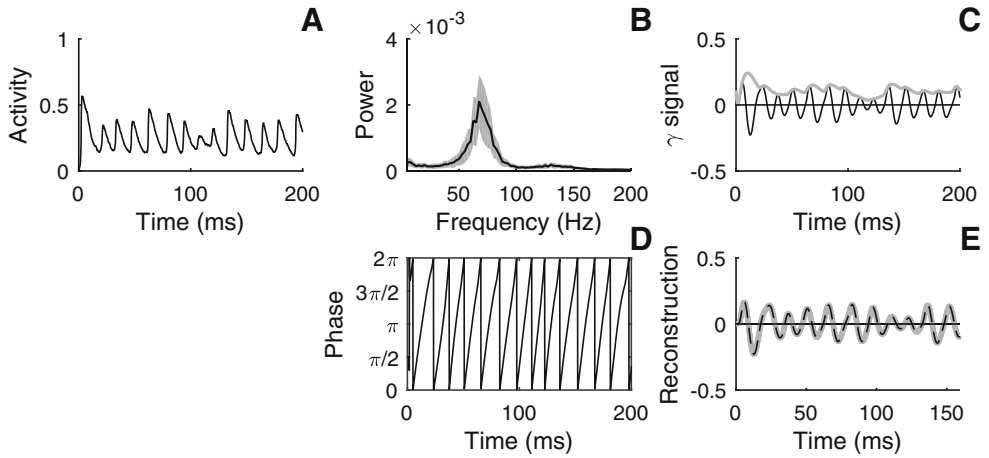


**Fig. 6** Illustration of the gamma phase extraction from full network simulations of the global activity. **a** Global activity as a function of time, i.e. the sum of I-activity and E-activity in the full network. **b** Power spectrum of the global activity. **c** Gamma ($\gamma$) part of the signal obtained by applying a bandpass filter (see Method) in the gamma band ($30 - 90$ Hz). The gamma signal oscillates around zero; the *grey line* is its envelope computed using the Hilbert transform (see Methods). **d** Phase of the $\gamma$-signal. **e** Superposition of the original gamma signal and of its Hilbert representation using the slow envelope and phase; the two are in excellent agreement. Parameters for the simulation are as in Fig. 5

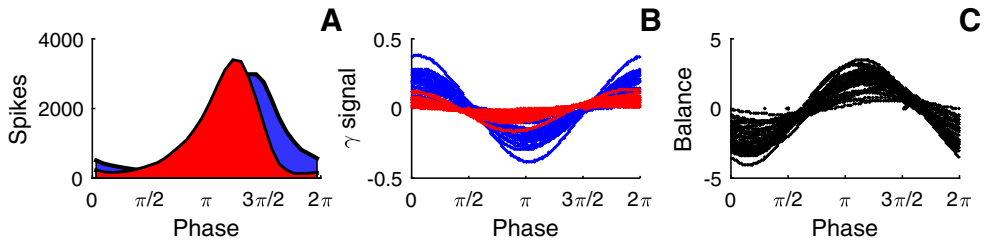


**Fig. 7** Illustration of the PING cycle and rhythmic modulation of the excitatory-inhibitory balance. **a** Proportion of neurons (E-cells in red and I-cells in *blue*) entering into the active state as a function of the ongoing phase of the endogenous gamma cycle, obtained by simulating the whole network. No external stimulation is applied here. These cycle histograms are constructed using 50 bins on the interval $(0, 2\pi)$. **b** The excitatory ($r_E$: *red line*) and inhibitory ($r_I$: *blue line*) components of the gamma rhythm produced by the stochastic Wilson-Cowan model (see Methods) of the whole network as a function of the ongoing gamma phase. Data from multiple successive cycles are superimposed. **c** The weighted balance of synaptic input $s_E$ to the pyramidal cells as a function of the gamma phase. For our neural network, the simulations in **b** and **c** were two orders of magnitude faster than those of the whole network; this speed-up factor depends on the number of neurons in the network. Again data from many successive cycles are superimposed. Parameters for the simulation are as in Fig. 5

where the synaptic inputs are

$$s_E(t) = w_{EE} r_E(t) - w_{EI} r_I(t) + h_E,$$

and

$$s_I(t) = w_{IE} r_E(t) - w_{II} r_I(t) + h_I.$$

and $f$ is the firing function. Moreover, it is also well-known that the Wilson-Cowan model exhibits a Hopf bifurcation. Thus, with finite-size fluctuations, the oscillatory regime of the cortical circuit is an emergent noisy limit cycle, as shown in the Methods section. This noisiness blurs any definition of phase for the emergent rhythm, thus impeding the determination of any window of firing opportunity.

### 3.2 Gamma phase and the window of opportunity

Cortical rhythms, and in particular gamma synchronization are thought to gate, select and suppress the flow of information between brain regions. To develop this argument requires going beyond the usual spectral analysis and explore the precise time evolution of the phase within a cycle and across cycles of the endogenous gamma rhythm; later we compute the window of opportunity using timed external pulses to a fraction of the E-cells. We computed the phase of the neural activity after the application of a bandpass filter that keeps only the gamma part (30-90 Hz) of the signal (see Fig. 6 and Methods). Our methodology illustrates how one can extract the ongoing phase (panel D) as well as the envelope (panel C) of the neural network activity in any oscillatory band of interest; a similar idea was used in (Greenwood et al. 2015) without this application of a bandpass filter. This enables us to investigate the information contained in the ongoing phase and/or envelope of any specific rhythm.

The core prediction of the CTC hypothesis is that the rhythmic inhibition during the gamma cycle gates the availability of pyramidal cells to respond to their own external excitatory input (as distinguished from their inhibitory input from the interneurons). The pyramidal cells will more likely fire when the inhibitory firing rate is low - although it is less clear whether this should occur in the waxing and/or waning phases of inhibition. Thus the rhythmic inhibition modulates the excitability of the E-cells, and thus their firing rate, allowing them to fire only during short windows of opportunity. If a pyramidal cell does not fire during this window in a given cycle, the cell has to wait until the next cycle. This is central to understand the

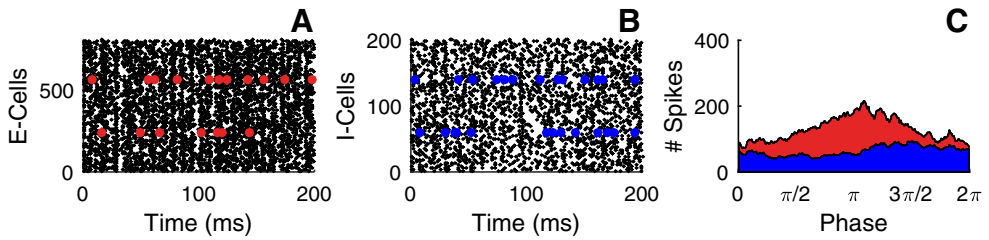


**Fig. 8** Illustration of the PING cycle and rhythmic modulation of the excitatory-inhibitory balance when the coupling among E-cells is non existant. **a** Raster plot depicting the spike timing for the E-cells. Similarly, **b** is the corresponding plot for the I-cells. **c** Proportion of neurons (E-cells in *red* and I-cells in *blue*) entering into the active state as a function of the ongoing phase of the endogenous gamma cycle, obtained by simulating the whole network. No external stimulation is applied here. These cycle histograms are constructed using 50 bins on the interval $(0, 2\pi)$. Parameters are the same as in Fig. 5 except the coupling among the E-cells $W_{ee}$ that is taken to be zero

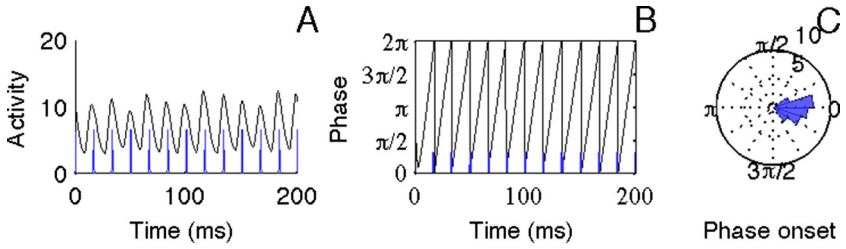


**Fig. 9** Illustration of the phase entrainment. **a** Global activity $r_E + r_I$ (*black line*) and external rhythmic drive on the I-cells (*blue line*). The simulation was made directly on the whole binary network. **b** Phase of the $\gamma$-signal (*black curve*); the blue pulses are the stimulus presentation times. **c** Histogram of phase of the global activity at the stimulus onset. Parameters are as in Fig. 5, except that the external drive to the I-cells is $Q_I = 0.3$ with $\sigma_I = 0.3$ and $f_I = 60$ as in Eq. (6)

observation made above (see in Fig. 5) where individual pyramidal cells spike only occasionally and miss several cycles (window of opportunity) before being able to fire again.

Figure 7 portrays the constituents of the gamma cycle and displays the temporal window. It shows in the first panel the precise spike timing of the onset of activity in E-cells and I-cells as a function of the gamma phase. A spike is associated with a neuron making a transition to the excited state. It is clear from this panel that the E-cells have a higher firing probability as the magnitude of the inhibition grows, rather than when it falls. The second panel displays the excitatory (red line) and inhibitory (blue line) gamma signal produced by the network. These are obtained from the stochastic Wilson-Cowan equations (see Methods), and correspond respectively to the variables $r_E(t)$ and $r_I(t)$. Simulation of these equations, as opposed to whole network simulations, yields a tremendous decrease in computation time (since it is independant to the number of cells present in the network) in order to obtain information on the phase dependence of the firing probability. These results also reveal that the inhibitory variability across cycles of the gamma rhythm is greater than the excitatory variability (see the spread of the blue vs red lines, respectively). This is expected from the shape of the stochastic limit cycle and associated excitatory and inhibitory time series shown in Fig. 2.

The third panel gives the total synaptic input $s_E$ to the pyramidal cells, made up of the weighted sum of the excitatory (E to E) and inhibitory (I to E) inputs. During a cycle, each pyramidal cell receives an input which is positive (depolarizing) during a short window (of opportunity) and negative (hyperpolarizing) otherwise. The rhythmic reverberation in the E-I network arises from the periodic modulation of the balance of inputs to the pyramidal cells, and consequently, of their firing probability. For the parameters chosen, one can see from the magnitudes that this firing modulation is principally due to the variation in the inhibition (Figs. 7b and 8). It makes good sense then to stabilize the gamma rhythm experimentally by driving the interneurons - rather than the pyramidal cells - with external periodic pulses, as in (Cardin et al. 2009). One would want to do that anyways if one wishes to avoid the interference of a rhythm-regularizing pacing stimulation with an external "communication" signal being later applied to the pyramidal cells.

The gamma cycle thus causes successive transitions between open and closed windows of excitability. Hence, one would expect the ongoing phase cycle to be a predictive measure of the pyramidal cell excitability (Fries 2005). As already stressed in the Introduction, this may subserve stimulus selection in attentional processes (Fries et al. 2007), which is the subject of the next section. The excitatory-inhibitory balance is constantly dynamical in nature in this system, as its shifts produce the gamma rhythm, and the openings and closings of the window. The external stimulation to the interneurons that we next explore serves to better understand how much phase matters in communication.

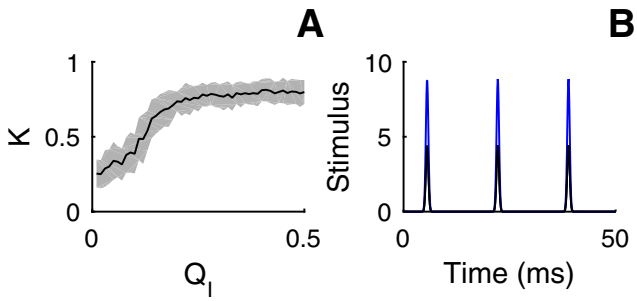


**Fig. 10** Measure of the entrainment of the global activity of the neural network to the external rhythmic drive (6). **a** Kuramoto index (7) of phase locking of the global activity (number of active E and I cells) as a function of the amplitude of pacing stimulation of the interneurons. The measure is computed using an average over 100 realizations. The *black line* denotes the mean and the shaded region is the confidence interval of $\pm 1$ standard deviation. Parameters for the simulation are as in Fig. 5, except that the external drive to the I-cells is $Q_I = 0.3$ with $\sigma_I = 0.3$ and $f_I = 60$ as in Eq. (6). **b** Illustration of the rhythmic drive for two different stimulation amplitudes $Q_I = 0.1$ (*black*) and $Q_I = 0.3$ (*blue*, used for the results in panel **a**)

### 3.3 Entrainment of the gamma rhythm

To deepen our dynamical understanding of the core prediction of the CTC hypothesis, we designed a follow-up series of numerical experiments in the spirit of Cardin et al. (2009). We start by artificially locking the fast basket cells to an external drive in order to stabilize the gamma rhythm. This will enable the definition of a precise phase, and consequently, the exploration of how "in principle", in this best scenario low-noise case, pyramidal cell responses to inputs external to the network depend on gamma phase (the network here now understood as E cells, plus I cells, plus pacing to the I cells). This will reveal basic information about the same question in the noisier E-I system without pacing. We use a rhythmic drive analogous to (Börgers and Kopell 2008). In this computational experiment, the external rhythmic drive mimics the periodic light-driven activation of fast-spiking interneurons in (Cardin et al. 2009).

The consequence of such a rhythmic drive is the entrainment of the gamma rhythm as illustrated in Fig. 9. Indeed, the histogram of the phases at the stimulus onset (peak of the external drive) shows a concentrated distribution around zero. Furthermore, to quantify this entrainment with respect to the stimulus, we computed the Kuramoto order parameter for Fig. 10. Originally, the Kuramoto index was introduced to measure the degree of synchrony among identical interacting oscillators. Here we use the Kuramoto parameter as a measure of phase locking (Lachaux et al. 1999), i.e. to quantify how tightly the global activity of the network (defined as the number of active E and I cells) is locked to the external periodic drive - or, in other words, how the global activity (defined as the number of active E and I cells ) of the network is entrained by the external pulses.

From its definition, the Kuramoto index is a value between zero and one, with a value close to zero for poor entrainment (weak phase locking), and close to one for strong entrainment (strong phase locking). As expected, increasing the amplitude of the stimulus that paces the I-cells induces a better entrainment of the gamma cycle. Now that the cortical circuit is entrained and its gamma cycle is more regular, we can easily investigate the interaction between external (e.g. sensory) stimuli to the pyramidal cells and the externally-regularized endogenous gamma rhythm.

The effect of the stimulation on the E and I cells is studied now via the power spectrum in Fig. 11. By pacing the E-cells alone, and then the I-cells alone, we observe strong effects on the power spectrum as the frequency of the external rhythmic drive is changed. To illustrate this, we have measured the peak amplitude of the power spectrum as a function of the frequency of the external drive. We clearly distinguish that the network reacts well to the drive when its frequency is close to the natural frequency of the neural network. To be precise, it has to be just a little bit below the natural frequency of the network.

Note finally that the information presented in Figs. 10 and 11 can also be computed by the direct simulation of the network as well as the simulation of the SDEs (5) presented in the Methods section, even though only results on the full network have been presented here due to lack of space (except for Figs. 7c and 12). Indeed, from simulation of the SDEs, one is able to quickly get all the statistical information of the network that does not require the precise dynamics of a particular cell. This is indeed the case when computing the Kuramoto coefficient as well as the power spectrum. The SDEs are also amenable to analytical

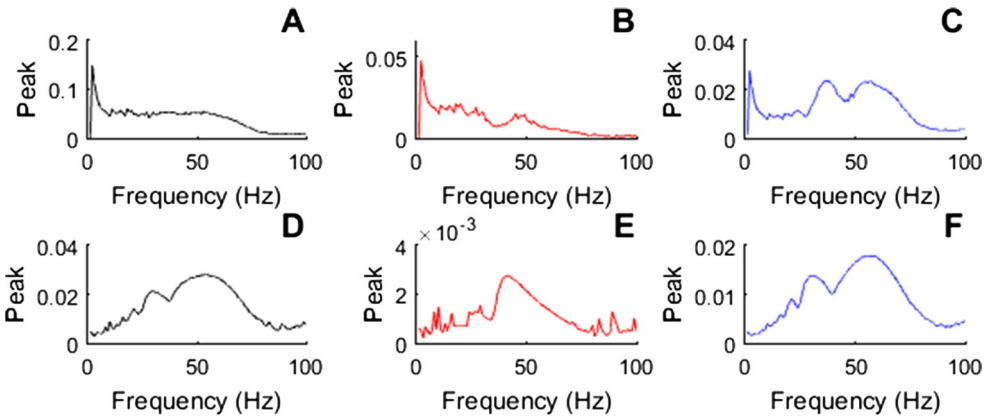


**Fig. 11** Illustration of the effect of the external pacing frequency on the power spectrum. The figure illustrates how the peak amplitude of the power spectrum depends on the frequency of the external drive. Parameters for the simulation are as in Fig. 5, and the external drive on I/E-cells uses $Q_I/Q_E = 0.3$, $\sigma_I/\sigma_E = 0.3$. In the panels **a-b-c** the pacing is made on the E-cells, while in the panels **d-e-f** the pacing is made on the I-cells. **a–d** Power spectrum of the global activity. **b–e** Power spectrum of the E-cells. **c–f** Power spectrum of the I-cells. These results were obtained from simulations of the two stochastic differential equations Eqs.(5) rather than of the whole network

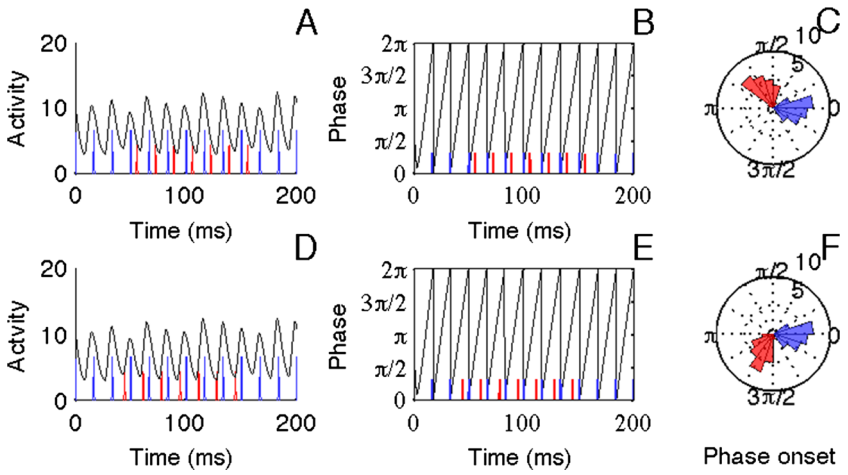


**Fig. 12** Gamma phase at the onset of stimulations to the E and I cells. **a** Time series of the global activity $r_E + r_I$ (*black line*) and of the two external rhythmic drives: one to the I-cells (*blue line*) and the other to the E-cells (*red line*). **b** Phase of the $\gamma$-signal (*black curve*); the blue pulses denote the onset of stimuli to the I-cells, while the red pulses are those to the E-cells. **c** Histogram representation of gamma phase at stimulus onset, in *blue* for the *blue* pulses and in *red* for the *red* pulses, where these stimulation phases are referenced to the phase of the global gamma rhythm. The simulations were made with the whole binary network. Panels **d-e-f** correspond respectively to panels **a-b-c** but are computed for a later phase. Parameters for the simulation are as in Fig. 5, and the external drive on I-cells uses $Q_I = 0.3$, $\sigma_I = 0.3$ and $f_I = 60$; the external drive on E-cells uses $Q_E = 0.2$, $\sigma_E = 0.3$ and $f_E = 60$. Panels **a-b-c** are for $\phi_E = 2\pi/3$, and panels **d-e-f** for $\phi_E = 5\pi/3$

investigations, which are beyond the scope of the present paper.

### 3.4 Excitability of the pyramidal cells

Most studies of gamma oscillations have so far focused on cortical circuits without external input. Yet to assess the impact of gamma oscillations on computational capabilities, interaction with external stimuli needs to be examined. According to the CTC hypothesis, if a stimulus is presented, the evoked response of the pyramidal cells should depend on the precise timing of the stimulus onset relative to the ongoing phase of the gamma cycle. More precisely, if a stimulus is presented at the peak of inhibition, CTC predicts a weak evoked response, and vice-versa. The rhythmic inhibition thus modulates the effectiveness of external stimuli to alter the firing of the pyramidal cells. To address this prediction, we follow the same strategy of (Cardin et al. 2009). We drive a small fraction (20 percent) of the pyramidal cells and measure their evoked response (number of spikes produced by this subpopulation) during 200 ms of simulation. We study this effect as a function of the shift of

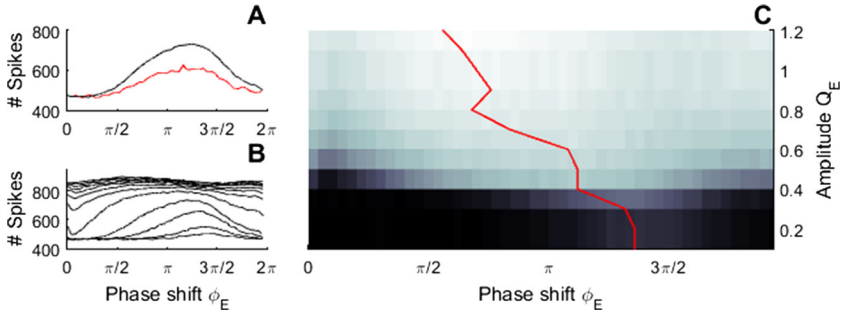


**Fig. 13** Dependence of the evoked response of the E-cells on the phase of the gamma rhythm and the amplitude of external stimulation to the E-cells. **a** Spike count emitted by the 50 pyramidal cells receiving the stimulus as a function of the phase shift $\phi_E$. This numerical result is obtained via an averaging over 100 simulations of 400 ms. In all our simulations, we use a time bin of 0.1 ms. The *black line* denotes the mean value and the shaded region represents a one standard deviation interval of confidence. Parameters for the simulation are as in Fig. 5, and the external drive on I-cells uses $Q_I = 0.3$, $\sigma_I = 0.3$ and $f_I = 60$; the external drive on E-cells uses $Q_E = 0.2$, $\sigma_E = 0.3$ and $f_E = 60$. The red curve corresponds to a pacing with a pulse arriving on the E-cells with a period two times slower than pulses on the I-cells, to see if slower pacing as in Cardin et al. alters our results. The shape of the curve is preserved, with the expected reduction in spike count by half. **b** Dependence of the E-cell excitability vs gamma phase relationship on the amplitude of the stimulus to the E-cells. **c** Same as B but in a colour-coded representation of excitability, the ordinate calibration shows 450 − 900, which corresponds to a number of spikes; the *red line* gives the optimal phase processing with respect to the stimulus amplitude

the periodic drive to the E-cells relatively to the pacing periodic drive to the I-cells (see Methods). In the true biological setting, such pulses to the E-cells would arise from a number of more or less synchronized EPSPs (Excitatory Post-Synaptic Potentials) from another population somewhere in the brain.

Note that it would have been very difficult to test the CTC prediction without artificially locking the gamma oscillator. We illustrate the precision of the phase target in Fig. 12. The circular histograms emphasize the design of our numerical experiment. They reveal the shift between phase onset of E-cell stimulation relative to phase onset of I-cell (pacing) stimulation.

Our crucial finding, in agreement with Cardin et al. (2009), is that the timing of the stimulus onset relative to the ongoing gamma cycle delicately governs the magnitude of the change in firing rate of the pyramidal cells. We plot in the first panel of Fig. 13 the number of action potentials produced by the subpopulation of excited cells as a function of the phase shift. As we clearly see, the evoked response (number of action potentials produced by the subpopulation during the simulation) strongly depends on the phase shift. Note that the presented stimuli are the same in every realization; the differences in the responses are solely due to the fluctuating intrinsic activity of the network (caused by the stochastic nature of the single neuron dynamics) and the ongoing phase.

To further investigate this dependency, we tested the influence of the amplitude of the stimulus as well (see the panels B and C in Fig. 13). This is meant to extend the CTC to the plausible situation where communication between networks involves both amplitude and phase information. The amplitude may vary due to e.g. to number of pre-synaptic external neurons firing at a given instant as they are contributing to their own local gamma rhythm; communication would then be best if that rhythm is at the same frequency as that of the PING network of interest. Our simulation interestingly reveals how the preferential phase (the phase with the stronger response) varies with respect to the external stimulus intensity. Indeed, for moderate stimuli, the response of the subpopulation can double if the stimulus arrives at the 'good' phase. On contrary, if the stimulus arrives at the 'wrong' phase, the input has difficulty to induce any response; in that case, one would deduce that the stimulus is not processed and that communication is poor.

The phase thus defines a relatively narrow window of opportunity for the processing of low to moderate inputs. However, when strong enough, the input dominates or "overrides" the inhibitory input, producing a response that depends much less on the phase. Hence, we see a clear trade-off between the amplitude of the response and its phase selectivity. In between, the peak of the window, and indeed its width, depend continuously on the amplitude of the stimulation to the E-cells. Generally, we also see that the preferred phase is a function of the magnitude of external stimulation. In a more natural situation where this magnitude fluctuates as the number of presynaptic neurons firing in any given cycle fluctuates, the best "communication" (in the sense of strongest postsynaptic effect) would occur at phases that also fluctuate. If the E-cell stimulation phase were somehow kept fixed, then the magnitude of the E-cell response would continually track the magnitude of the presynaptic stimulus. The communication could then be done with both constant phase and amplitude or, perhaps more efficiently, with time-varying phase and amplitude.

Thus, by its intrinsic constitution, the gamma cycle defines a narrow window of opportunity for the processing of moderate inputs. However, this is strongly sensitive to noise and to the entrainment of the I-cells. As illustrated in Fig. 14, when the phase target is no longer precise and small fluctuations deviate the phase stimulus onset (see Fig. 3), the evoked response of the pyramidal cells loses its phase dependence. Noise flattens the evoked response and diminishes the phase preference. Hence, a strong precision in the phase target is needed in order to be better processed.

In a similar spirit, we tested the excitability of the pyramidal cells with respect to phase as a function of the level of synchronization of the I cells. This level was modified

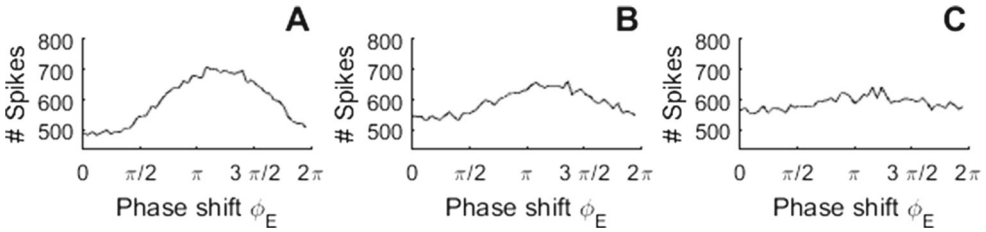


**Fig. 14** Illustration of the influence of noise in the phase target. The figure illustrates the dependence of the evoked response of the E-cells with respect to the phase of the gamma rhythm at which the stimulus is presented. Spike count emitted by the 50 pyramidal cells receiving the stimulus as a function of the phase shift $\phi_E$. This numerical result is obtained via an averaging over 100 simulations of 400 ms. In all our simulations, we use a time bin of 0.1 ms. The *black* line denotes the mean value and the shaded region represents a one standard deviation interval of confidence. Parameters for the simulation are as in Fig. 5, and the external drive on I-cells uses $Q_I = 0.3, \sigma_I = 0.3$ and $f_I = 60$; the external drive on E-cells uses $Q_E = 0.3, \sigma_E = 0.3$ and $f_E = 60$. **a** $\sigma_\eta = 0.1$. **b** $\sigma_\eta = 0.2$. A) $\sigma_\eta = 0.3$

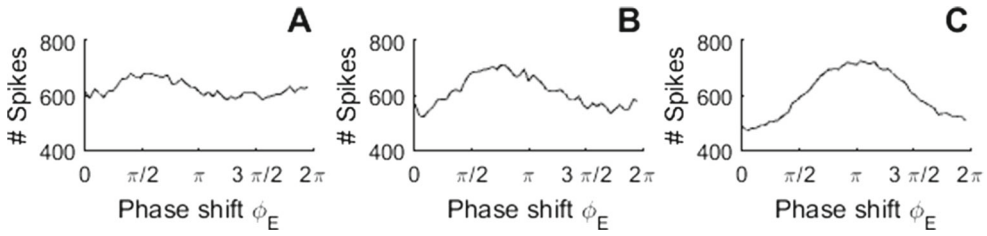


**Fig. 15** Illustration of the influence entrainment on the phase excitability. The figure illustrates the dependence of the evoked response of the E-cells with respect to the phase of the gamma rhythm at which the stimulus is presented. Spike count emitted by the 50 pyramidal cells receiving the stimulus as a function of the phase shift $\phi_E$. This numerical result is obtained via an averaging over 100 simulations of 400 ms. In all our simulations, we use a time bin of 0.1 ms. The *black* line denotes the mean value and the shaded region represents a one standard deviation interval of confidence. Parameters for the simulation are as in Fig. 5, and the external drive on I-cells uses $\sigma_I = 0.3$ and $f_I = 60$; the external drive on E-cells uses $Q_E = 0.3$, $\sigma_E = 0.3$ and $f_E = 60$. A) $Q_I = 0.1$ B) $Q_I = 0.15$ A) $Q_I = 0.2$

by changing the strength of the entraining stimulation to the I cells. As we can see in Fig. 15, by increasing the pulse amplitude on the I-cells $Q_I$, the peak of excitability shifts and the amplitude (max-min) of the curves also increases. This means that the stronger the I-cells are locked, the more the response of the E-cells is phase dependent.

## 4 Discussion

Despite extensive research, there is still no concensus on the potential cognitive functions of rhythmic oscillations in the brain (Buzsàki 2006). One widely accepted hypothesis states that those oscillations regulate the flow of information across brain regions (Sejnowski and Paulsen 2006). This hypothesis was partially already confirmed (Fries et al. 2007) even if some criticisms were raised (Rolls et al. 2012). In fact, for attentional process, stimulus selection and signal discriminability, a number of studies have suggested that rhythmic synchronization in the gamma-frequency band acts as a top-down processing to modulate sensory input and select the attended stimulus (Fries 2005); see also (Tiesinga 2012) for a discussion of PING vs ING, and (Akam and Kullmann 2014) for another theory of communication across cortical regions.

Here we looked at the stochastic dynamical basis of this hypothesis. Toward this end, we used computational modeling and a novel fast numerical simulation method (based on networks of noisy two-state neurons) to replicate certain results of Cardin et al. (2009) and investigate how fluctuations shape the phase dependence. Cardin et al. (2009) showed that the gamma cycle admits optimal phases that regulate the response of E cells, and our simple stochastic model reproduces this empirical observation. We found that the phase dependence, and consequently the CTC hypothesis per se, to be sensitive to fluctuations. It exhibits a mild robustness to noise, since increasing jitter in the timing of inputs as well as gamma rhythm irregularity both tend to wash out the phase dependence. Further, the phase at which the stimulation of the E cells optimally elicits responses depends on the synchrony of the I cells - proportional to the amplitude of the external pulses that entrain them - and on the amplitude of the E-cell stimulation. There is just a mild remnant of the phase dependence when the gamma rhythm is weakly entrained, which raises the issue of the extent of the CTC viability in the absence of artificial entrainment. The weak phase dependence under "natural" conditions may nevertheless be observable through population averaging. It may also be that an ING type mechanism, rather than the PING one studied here, could endow more robustness to the CTC if the inhibitory interactions yield a highly stable gamma rhythm to feed to the E cells.

As we have seen, the neural mechanism underlying the gamma rhythm, and especially its rhythmic inhibitory feedback, is naturally suited for stimulus suppression. Only the input that is sent around the peak of excitability will be processed in the sense of having an impact on E-cell firing rate, while the others will be suppressed. Therefore, by exposing the underlying dynamics, our findings support the potential role of gamma band synchronization in attentional process. Our results further show that the interneurons exhibit stronger cycle-to-cycle fluctuations than the pyramidal cells for the generic circuit configuration and parameters we have used. Light pulses to these interneurons thus have a strongly stabilizing effect on the gamma rhythm, endowing it with a more regular phase.

Our approach complements recent computational studies that aimed to reproduce certain aspects of the Cardin et al. results (Tiesinga and Sejnowski 2010; Knoblich et al. 2010). Among other results, the first showed how constant and pulse inputs can shift the local field potentials between neural populations. Also, the computer-intensive detailed Hodgkin-Huxley model by Knoblich et al. (2010) has reproduced many of these aspects. But no analytical insight is available from such a detailed formalism. Further, while it introduces Poisson inputs to model cells to mimic cortical

variability, it does not examine the role of intrinsic and input timing variability in shaping CTC, as we have here.

On another note, the stochastic Wilson-Cowan (WC) model used here produces spike times that can be tracked numerically. It converges to the deterministic WC firing rate model in the infinite neuron limit. However, this model does not produce autonomous oscillations in the absence of recurrent excitation (see Ermentrout and Terman 2010, p.351). There is debate in the literature as to whether recurrent excitation (E-E connections) is a necessary component of the PING mechanism. Most studies include such connections, such as the theoretical one that inspired our study (Wallace et al. 2011), and is seen in various reviews (Buzsáki and Wang 2012; Tiesinga 2012; Brunel and Hakim 1999), but some do not (e.g. Cannon et al. 2014). This led us to briefly investigate (Fig. 9) the effect of removing the EE connections. In this case the rhythm is completely dependent on the noise, i.e. it is induced by the finite size effects - as opposed to the main part of our results where the system exhibited oscillations even in the noiseless infinite neuron limit (i.e. it was above the Hopf bifurcation for the chosen parameters as in Wallace et al. 2011). This means that in principle the CTC does not need a gamma rhythm with a deterministic backbone to be operational: the CTC is also compatible with noise-induced rhythms.

The experiments of Cardin et al. (2009) which motivated our study lends support to the CTC hypothesis. As a side comment, the authors suggest that their results are slightly more supportive of the ING (Interneuron Network Gamma) mechanism of gamma rhythm generation rather than PING. The ING mechanism can be seen as simpler because the rhythm does not depend on the pyramidal cells; rather it arises solely from interactions between I-cells. The E-cells are simply receiving this stimulation, and their activity does not affect the I-cell rhythm. In the context of the Cardin et al. experiment, the optogenetic stimulation of the I-cells amounts to a regularization of this I-cell-based endogenous rhythm. This result is rather trivial to reproduce; this is also the case for the firing probability of an E-cell to an external excitatory pulse as a function of the phase of the inhibitory drive at which this pulse arrives (not shown). Given the ongoing debate about ING vs PING, we have chosen to address the PING scenario, in which the rhythm involves the interaction of both E and I-cell populations and where external pulses to the E-cells have the potential to also disrupt the cycle. In this case the rhythm has less phase coherence. Our results nevertheless show that Cardin's main results are also compatible with a PING mechanism.

We have found that there is a trade-off between the phase selectivity of the E-cells - measured e.g. by the width of the window of opportunity - and their firing rate. Cells in a network oscillating at the same frequency as the gamma rhythm in the E-I network of interest will be able to modulate the pyramidal cell activity, and thus "communicate", although the phase selectivity becomes irrelevant as the amplitude of that stimulus increases (e.g. as the number of firing pre-synaptic neurons increases). Further experiments are needed to determine the biophysical significance of this trade-off for the further development of CTC theory. They are expected to show that the peak and width of the window are indeed controlled by the amplitude of the external stimulation, and hopefully will offer insight for the significance of these quantities for communication purposes. It also remains to be seen how a time-varying amplitude of a presynaptic stimulus to the E-cells translates into a time-varying probability of E-cell firing, given the dependence of phase preference on stimulus amplitude.

Similarly, the window of opportunity is clearly shaped by the precision of the timing of the pulses to the E cells. Indeed, we have seen that a strong precision in the phase target is needed in order to modulate the evoked response, and the noise jitter rapidly washes out this modulation effect. In contrast, this jitter does not shift the peak of the phase dependence. Another interesting effect is the impact of the I-cells locking. We have indeed observed that the amplitude (max-min) of the modulation also increases as the phase locking of the I-cells increases; the position of the peak and overall shape of the phase dependence are sensitive to this pacing. For weak pacing, a weak phase dependence survives, but this certainly weakens the overall appeal of the CTC mechanism unless other rhythm stabilizing forces or population averaging effects come into play.

We have also looked at how the spectral peak in the individual and combined activities of the E and I cells changes with the frequency of the pacing (Fig. 12). This was done by pacing only the E cells, and only the I cells. Although our measure slightly differs from that of Cardin et al. (we do not normalize), we see that the E cells do not show a resonance when we sweep through the frequency at which they are stimulated - even though the I cells do. Further, a resonance is clearly observed for all three activities if the I cells are stimulated. Thus our stochastic PING model suggests that the gamma rhythm is more effectively maintained through pacing of the I cells. It would also be interesting in the future to extend the stochastic model used here to explicitly incorporate synaptic response time scales. The neural time scales $\alpha_E^{-1}$ and $\alpha_I^{-1}$ are only loosely tied to such synaptic time scales, since they respectively determine how the activities in the E and I populations return to equilibrium. And the time constants $\beta_E^{-1}$ and $\beta_I^{-1}$ are tied to the strength of the coupling of a cell to its inputs. Thus we can not easily quantify the role of synaptic time scales in the effects reported here, e.g. which ones are crucial for the genesis of the gamma rhythm. This makes our results nevertheless relevant to rhythms in general, but slightly weakens their

direct specificity to gamma rhythms. Likewise incorporating delays in the framework could be done to see their effect, as in (Dumont et al. 2014) for nets of inhibitory cells.

Our results generally support the notion that the current state of a cortical circuit affects the input effectiveness. The evoked response is consequently given by an interaction between the internally generated activity and an external stimulus. Our results highlight this interaction and disentangle the intricate relationship between the response, the ongoing gamma phase and the amplitude of the input. This is crucial for stimulus suppression in attentional process. Furthermore, our results give a better understanding of how a good phase relation could enhance information transfer (see Womelsdorf et al. 2007; Buehlmann and Deco 2010), in spite of internal and external sources of fluctuation.

Large response variability to identical stimuli is commonly reported in the literature. This trial-to-trial variability remains incompletely understood and is mainly imputed to noise. Our computational modelling approach points to another potential candidate: the phase of ongoing activity in different frequency bands. Due to ongoing fluctuating internal rhythms, gamma and non-gamma, the network can be in different states (e.g. gamma phase) when a stimulus arrives, producing different responses to similar inputs. Understanding this interaction and in particular its dependence on the amplitude and frequency of both the stimulus and current brain state remains an interesting avenue to explore.

In the future it would also be of interest to test another prediction of the CTC., such as the precise way in which different stochastic neuron groups interact with a given target and compete to convey information to it. The CTC hypothesis states that an enforcement of gamma power is sufficient to entrain its target and then convey its information. One would need to investigate if an increase of gamma power is sufficient to boost the level of transmitted information between a certain neural group and its target, and what effect the frequency mismatch may have. Likewise, the regulation of the information transmission by the balance of excitation and inhibition in pathology is another potential avenue to explore with the formalism and fast simulation techniques presented here, which incorporates directly the stochastic emergent nature of the rhythms.

**Acknowledgments** This work was supported by the Natural Sciences and Engineering Research Council of Canada (AL) and the University of Ottawa Research Chair in Neurophysics (AL). G.N. thanks CIHR (Canadian Institute of Health Research), the Michael Smith Foundations EJLB-Michael Smith Chair program, and the Hope for Depression Research Foundation (HDRF) for support.

**Conflict of interests** The authors declare that they have no conflict of interest.

## References

Akam, T., & Kullmann, D.M. (2014). Oscillatory multiplexing of population codes for selective communication in the mammalian brain. *Nature Reviews Neuroscience*, *14*, 111–122.

Bartos, M., Vida, I., & Jonas, P. (2007). Synaptic mechanisms of synchronized gamma oscillations in inhibitory interneuron networks. *Nature Reviews Neuroscience*, *8*, 45–56.

Benayoun, M., Cowan, J.D., van Drongelen, W., & Wallace, E. (2010). Avalanches in a stochastic model of spiking neurons. *Plos Computational Biology*, *6*(6), e1000,846.

Boashash, B. (1992). Estimating and interpreting the instantaneous frequency of a signal. ii. algorithms and applications. *Proceedings of the IEEE*, *80*(4), 540–568.

Börgers, C., & Kopell, N. (2008). Gamma oscillations and stimulus selection. *Neural Computation*, *20*(2), 383–414.

Bressloff, P.C. (2009). Stochastic neural field theory and the system-size expansion. *SIAM Journal of Appllied Mathematics*, *70*(5), 1488–1521.

Bressloff, P.C. (2010). Metastable states and quasicycles in a stochastic wilson-cowan model of neural population dynamics. *Physical Review E*, *82*(5), 051,903.

Bressloff, P.C., & Newby, J.M. (2013). *Metastability in a stochastic neural network modeled as a velocity jump markov process. Preprint (submitted).*

Brosch, M., Budinger, E., & Scheich, H. (2002). Stimulus-related gamma oscillations in primate auditory cortex. *Journal Neurophysiology*, *87*(6), 2715–25.

Brunel, N. (2000). Dynamics of sparsely connected networks of excitatory and inhibitory spiking neurons. *Journal of Computational Neuroscience*, *8*, 183–208.

Brunel, N., & Hakim, V. (1999). Fast global oscillations in networks of integrate-and-fire neurons with low firing rates. *Neural Computation*, *11*(7), 1621–1671.

Buehlmann, A., & Deco, G. (2010). Optimal information transfer in the cortex through synchronization. *Plos Computational Biology*, *6*(9), e1000,934.

Buice, M.A., & Chow, C.C. (2013). Dynamic finite size effects in spiking neural networks. *Plos Computational Biology*, *9*(1), e1002,872.

Buice, M.A., & Cowan, J.D. (2007). Field-theoretic approach to fluctuation effects in neural networks. *Physical Review E*, *75*(5), 051,919.

Buzsàki, G. (2006). *Rhythms of the Brain*: Oxford University Press.

Buzsáki, G., & Wang, X.J. (2012). Mechanisms of gamma oscillations. *Annual Review of Neuroscience*, *35*(10), 203–225.

Cannon, J., McCarthy, M., Lee, S.J., Börgers, C., Whittington, M., & Kopell, N. (2014). Neurosystems: brain rhythms and cognitive processing. *European Journal of Neuroscience*, *39* (5), 705–719.

Cardin, J., Carlén, M., Meletis, K., Knoblich, U., Zhang, F., Deisseroth, K., Tsai, L., & Moore, C. (2009). Driving fast-spiking cells induces gamma rhythm and controls sensory responses. *Nature*, *459*(7247), 663–7.

Csicsvari, J., Jamieson, B., Wise, K., & Buzsáki, G. (2003). Mechanisms of gamma oscillations in the hippocampus of the behaving rat. *Neuron*, *37*(2), 311–22.

Dumont, G., Northoff, G., & Longtin, A. (2014). Linear noise approximation for oscillations in a stochastic inhibitory network with delay. *Physical Review E*, *90*(1).

Rolls, E.T., Webb, T.J., & Deco, G. (2012). Communication before coherence. *European Journal of Neuroscience*, *36*, 2689–2709.

Engel, A.K., Kreiter, A.K., König, P., & Singer, W. (1991). Synchronization of oscillatory neuronal responses between striate and extrastriate visual cortical areas of the cat. *Proceedings of the*

*National Academy of Sciences of the United States of America*, *88*(14), 6048–6052.

Ermentrout, B., & Terman, D. (2010). *Mathematical foundations of neuroscience*: Springer.

Fries, P. (2005). A mechanism for cognitive dynamics: neuronal communication through neuronal coherence. *Trends Cognitive Science*, *9*(10), 474–80.

Fries, P., Nikolić, D., & Singer, W. (2007). The gamma cycle. *Trends Neuroscience*, *30*(7), 309–16.

Fries, P., Reynolds, J., Rorie, A., & Desimone, R. (2001). Modulation of oscillatory neuronal synchronization by selective visual attention. *Science*, *291*(5508), 1560–3.

Gillespie, D.T. (2001). Approximate accelerated stochastic simulation of chemically reacting systems. *Journal of Chemical Physics*, *115*(4), 1716–36.

Gillespie, D.T. (2007). Stochastic simulation of chemical kinetics. *Annual Review of Physical Chemistry*, *58*, 35–55.

Ginzburg, I., & Sompolinsky, H. (1994). Theory of correlations in stochastic neural networks. *Physical Review E*, *50*(4), 3171–3191.

Greenwood, P.E., McDonnell, M.D., & Ward, L.M. (2015). Dynamics of gamma bursts in local field potentials. *Neural Computation*, *27*(1), 74–103.

Grytskyy, D., Diesmann, T.T.M., & Helias, M. (2013). A unified view on weakly correlated recurrent networks. *Frontiers Computational Neuroscience*, *7*, 131.

Helias, M., Tetzlaff, T., & Diesmann, M. (2014). The correlation structure of local neuronal networks intrinsically results from recurrent dynamics. *Plos Computational Biology*, *10*(1), e1003,428.

Knoblich, U., Siegle, J.H., Pritchett, D.L., & Moore, C.I. (2010). What do we gain from gamma? local dynamic gain modulation drives enhanced efficacy and efficiency of signal transmission. *Front Hum Neurosci*, *21*(4).

Kukjin Kang, M.S., Henrie, J.A., & Shapley, R. (2010). Lfp spectral peaks in v1 cortex: network resonance and cortico-cortical feedback. *Journal of Computational Neuroscience*, *29*(3), 495–507.

Lachaux, J., Rodriguez, E., Martinerie, J., & Varela, F. (1999). Measuring phase synchrony in brain signals. *Human Brain Mapping*, *8*(4), 194–208.

Lindner, B., Doiron, B., & Longtin, A. (2005). Theory of oscillatory firing induced by spatially correlated noise and delayed inhibitory feedback. *Physical Review E*, *72*(2), 061,919–061,933.

Mazzoni, A., Panzeri, S., Logothetis, N., & Brunel, N. (2008). Encoding of naturalistic stimuli by local field potential spectra in networks of excitatory and inhibitory neurons. *Plos Computational Biology*, *4*, e1000,239.

Northoff, G. (2014). *Unlocking the Brain, Volume 1: Coding*: Oxford University Press.

Renart, A., de la Rocha, J., Bartho, P., Hollender, L., Parga, N., Reyes, A., & Harris, K.D. (2010). The asynchronous state in cortical circuits. *Science*, *327*(5955), 587–590.

Salinas, E., & Sejnowski, T. (2001). Correlated neuronal activity and the flow of neural information. *Nature Reviews Neuroscience*, *2*(8), 539–50.

Schoffelen, J., Oostenveld, R., & Fries, P. (2005). Neuronal coherence as a mechanism of effective corticospinal interaction. *Science*, *308*(5718), 111–3.

Sejnowski, T., & Paulsen, O. (2006). Network oscillations: emerging computational principles. *Journal of Neuroscience*, *26*(6), 1673–6.

Stopfer, M., Bhagavan, S., Smith, B., & Laurent, G. (1997). Impaired odour discrimination on desynchronization of odour-encoding neural assemblies. *Nature*, *390*(6655), 70–4.

Tiesinga, P. (2012). Motifs in health and disease: the promise of circuit interrogation by optogenetics. *European Journal of Neuroscience*, *36*(2), 2260–72.

Tiesinga, P., & Sejnowski, T. (2009). Cortical enlightenment: are attentional gamma oscillations driven by ing or ping? *Neuron*, *63*, 727–732.

Tiesinga, P.H., & Sejnowski, T.J. (2010). Mechanisms for phase shifting in cortical networks and their role in communication through coherence. *Front Hum Neurosci*, *4*(196).

Tiesinga, P.H.E. (2012). Motifs in health and disease: the promise of circuit interrogation by optogenetics. *European Journal of Neuroscience*, *36*(2).

Wallace, E. (2010). A simplified derivation of the linear noise approximation. arXiv:1004.4280.

Wallace, E., Benayoun, M., van Drongelen, W., & Cowan, J.D. (2011). Emergent oscillations in networks of stochastic spiking neurons. *Plos one*, *6*(5), e14,804.

Wallace, E., Gillespie, D.T., Sanft, K.R., & Petzold, L.R. (2013). *A new perspective on the linear noise approximation*. Preprint (submitted).

Wang, X., & Buzsáki, G. (1996). Gamma oscillation by synaptic inhibition in a hippocampal interneuronal network model. *Journal of Neuroscience*, *16*(20), 6402–13.

Wilson, H.R., & Cowan, J.D. (1972). Excitatory and inhibitory interactions in localized populations of model neurons. *Biophysical Journal*, *12*(1), 1–24.

Womelsdorf, T., Schoffelen, J., Oostenveld, R., Singer, W., Desimone, R., Engel, A., & Fries, P. (2007). Modulation of neuronal interactions through neuronal synchronization. *Science*, *316*(5831), 1609–12.